SEMI-ANNUAL TECHNICAL REPORT

HIGH-RESOLUTION GAMMA-RAY SPECTROSCOPY STUDY

CONTRACT N00014-69-C-0372

Contractor:	Lockheed Missiles & Space Company
Project Leader:	Dr. W. L. Imhof (415) 324-3311, Extension 45595
Effective Date of Contract:	28 April 1970
Contract Expiration Date:	29 November 1970
Amount of Contract:	CPFF $248,235

Sponsored by Advanced Research Projects Agency
ARPA Order No. 1404

SEMI-ANNUAL TECHNICAL REPORT

CONTRACT NOOO14-69-C-0372

HIGH-RESOLUTION GAMMA-RAY SPECTROSCOPY STUDY

In the laboratory program, runs have just been completed with the newly acquired Pu^{239} targets for bombardments with thermal neutrons and with neutrons of energies 0.050, 0.419, 5 and 15.4 MeV. For U^{235} additional gamma-ray spectra have been measured as a function of time for neutron bombardments at the following energies: thermal, 0.050, 0.419, 0.521, 0.618, 0.713, 0.810, 0.904 and 0.998 MeV. These new sets of runs at several different neutron energies have all been performed for 40-minute bombardment durations followed immediately by 20 or more counting periods for total durations of ten to twenty hours. The neutrons were produced on the Lockheed 3-MeV Van de Graaff accelerator by the $H^2(d,n)He^3$, $H^3(d,n)He^4$ and $Li^7(p,n)Be^7$ reactions. Thermal neutrons were produced by the $Li^7(p,n)Be^7$ reaction with the addition of large quantities of paraffin moderator. In all cases, the neutron fluences incident on the target were measured with activation foils of Au, Ni or Al, the choice being dependent upon the neutron energy.

A preliminary analysis of the foregoing data has been performed with the objective of finding gamma-ray lines which exhibit significant variations in production rate with neutron energy and/or target isotope. The fission debris spectra from U^{235} and Pu^{239} are basically rather similar with some significant differences, as illustrated in Figure 1 for bombardment with thermal neutrons. This presentation represents only a portion of the energy range covered in the gamma-ray measurements. In the selected interval there is little contribution from gamma rays naturally emitted from either target. A more quantitative demonstration of the number and magnitudes of the differences in the areas of the various gamma-ray lines is shown in Figure 2. Here is plotted the differential distribution in the ratios of the intensities of the more intense lines of Pu^{239} and U^{235} to the intensities of the 1260-keV line in I^{135}. The intensities represent areas under the photopeaks as derived with the previously described peak-fitting computer program. One can see that many of the gamma lines display

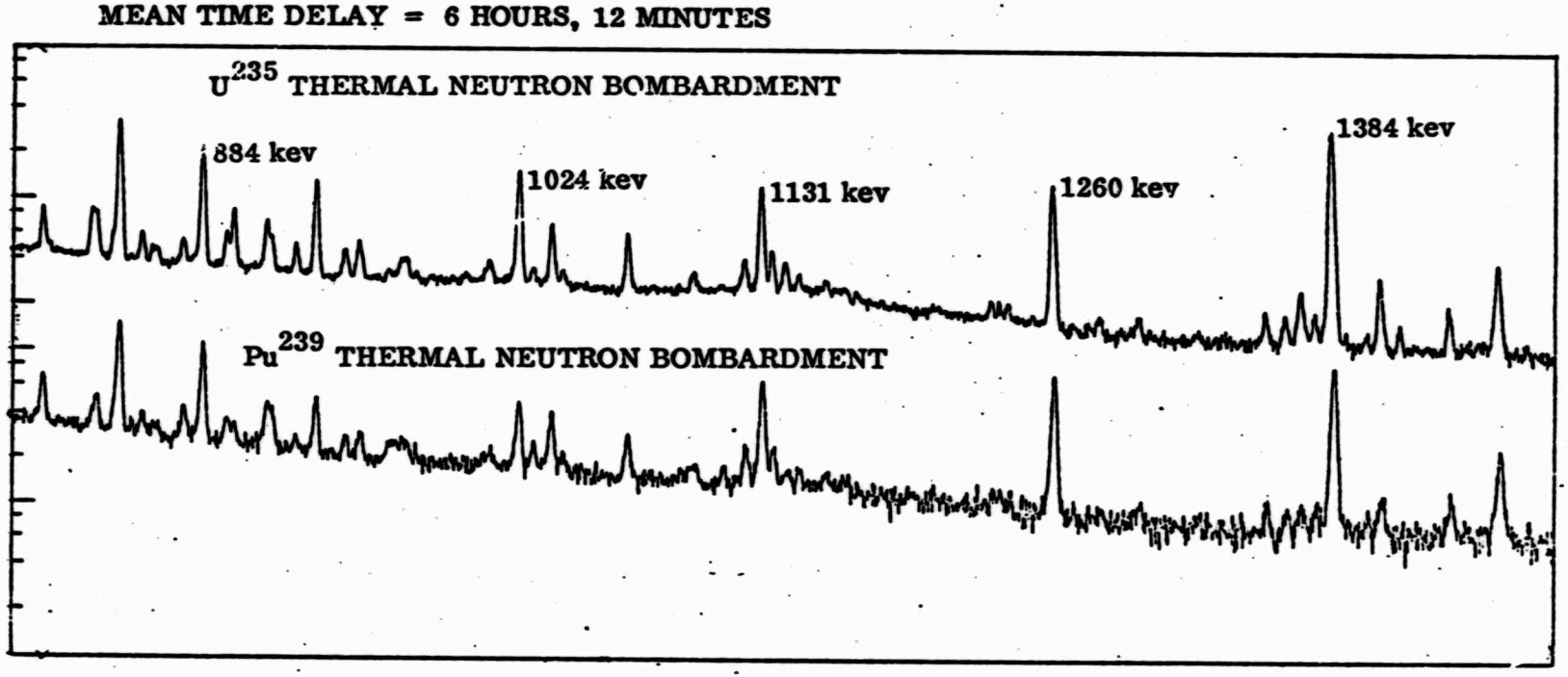

Figure 1 Portions of the gamma-ray spectra measured for the fission debris products from thermal neutron bombardments of U^{235} and Pu^{239}.

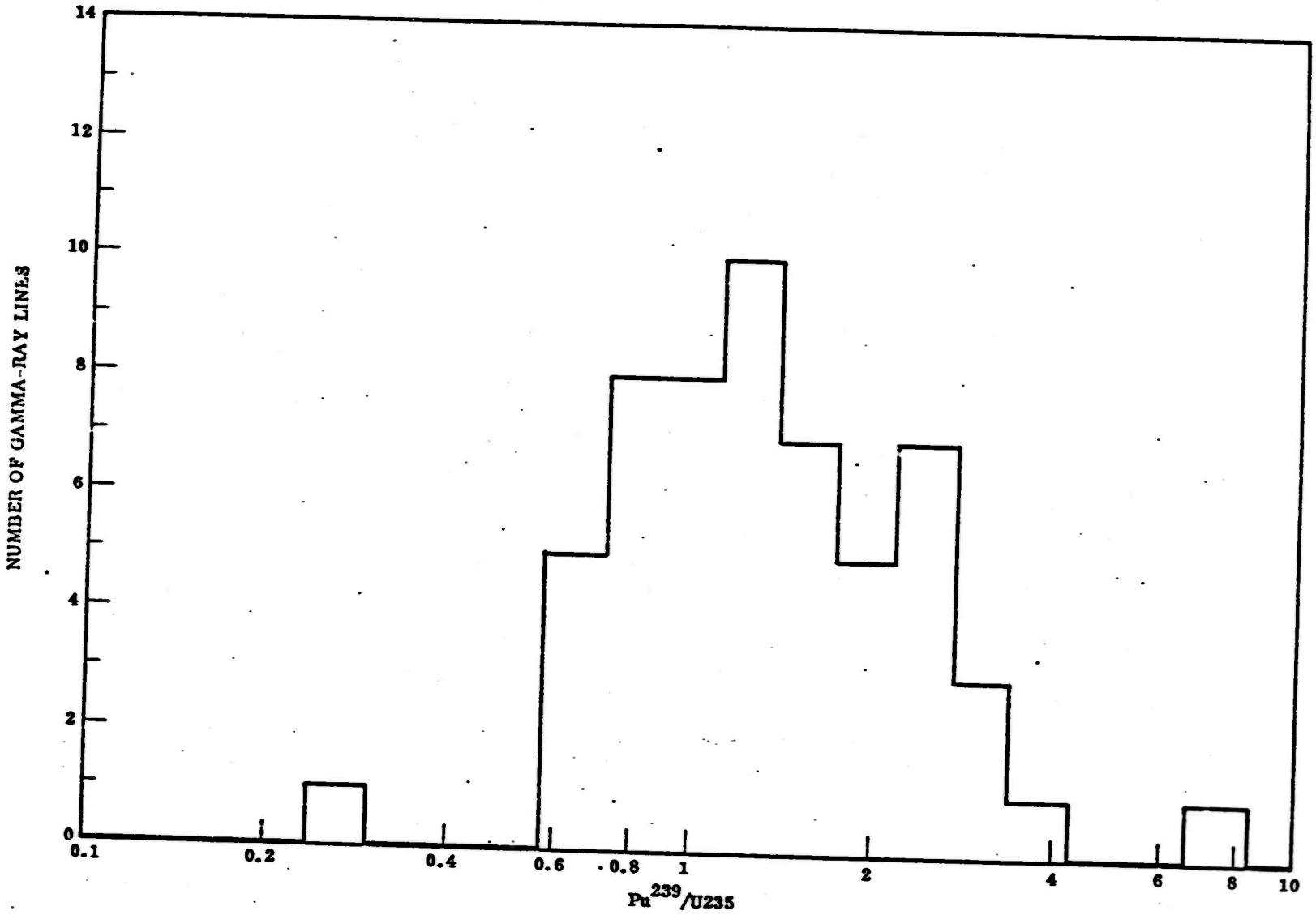

Figure 2 The differential distribution in the ratios of the intensities of the more intense lines of Pu^{239} and U^{235} each normalized to the intensity of the 1260-keV line in I^{135} for bombardments with 521-keV neutrons.

variations in relative intensity of the order of a factor of 2, depending upon whether the fissioning isotope is U^{235} or Pu^{239}. Therefore, although few dramatic differences exist between the gamma-ray spectra from the gross fission products of U^{235} and Pu^{239}, there are many significant variations in the more intense lines. Identification of the fissionable isotope from high-resolution gamma-ray measurements thus appears to be feasible. An analysis effort is currently underway to select those gamma-ray lines which best fulfill this objective for the satellite measurements. The 725-keV line from Ru^{105} is an example of a gamma ray whose intensity relative to that of the other gamma rays is strongly dependent (by a factor of more than 5) upon whether the fissionable isotope is U^{235} or Pu^{239}.

From the neutron bombardments of U^{235} at eleven different energies studies have been made of the variations with energy in the relative yields of the different gamma-ray lines. Some representative ratios are presented in Figure 3. It is seen that certain lines such as the 753-keV and 317-keV lines of Sn^{128} increase significantly with increasing neutron energy, whereas other lines show a decrease. These variations are being studied in more detail with particular emphasis on small but significant variations with neutron energy in the intensities of some of the more prominent lines. As described in previous reports identifications of the isotopes emitting the selected gamma rays are being made on the basis of the measured energies, the half-life values derived from the least squares fit routine, and available information concerning branching ratios.

Investigations have been made of the ability to discern altitude distributions of fission debris products from high-resolution gamma-ray measurements made from a satellite. Much of this study has been based on the previously described laboratory measurements of gamma-ray scattering and attenuation performed in large blocks of solid CO_2. These measurements were made with a Ge(Li) detector placed outside of various thicknesses of CO_2 surrounding a U^{235} foil previously irradiated in a reactor. As shown previously, the line shapes are not significantly distorted by the presence of the simulated atmosphere. However, the relative peak heights of the different energy gamma rays are affected, the measured attenuations agreeing well with those calculated from published cross sections.

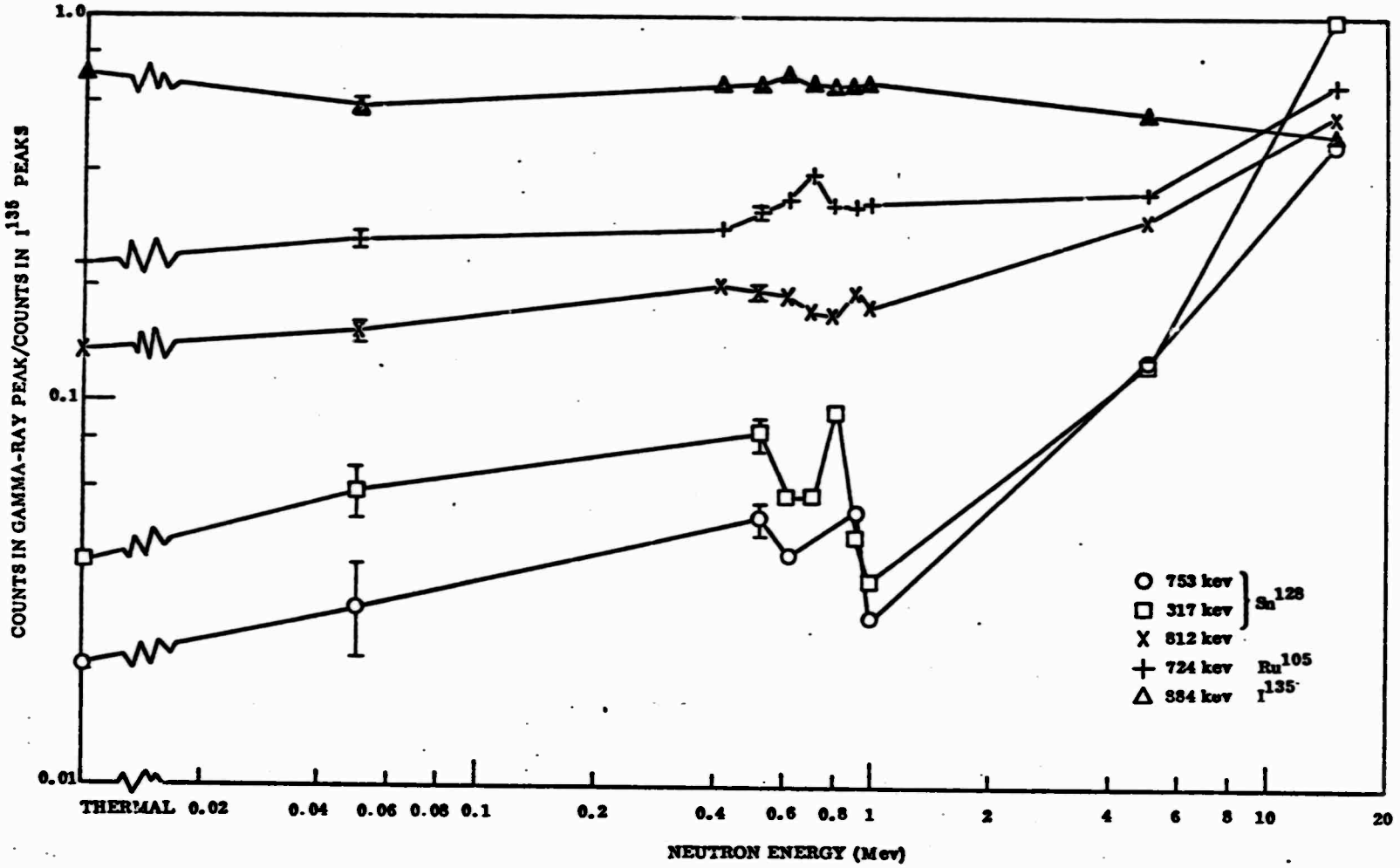

Figure 3. Ratios of the intensities of various gamma-ray peaks to the sums of the intensities of the I^{135} peaks at 1038, 1131 and 1260 keV plotted as a function of neutron energy.

An investigation has been made of the possible methods of using these variations to unfold fission debris altitude distributions. For this purpose we have considered isotopes (with suitable half-lives) which emit at sufficient intensities several gamma rays of widely differing energies. From the measured relative intensities of these different lines one can derive information on the altitude distributions. As an illustrative example, consider six of the more prominent gamma-ray lines emitted from the Te^{132}-I^{132} parent-daughter sequence. These gamma rays have energies of 229, 524, 668, 773, 955 and 1400 keV. In Figure 4 the normalized intensities fall off with energy exponentially in μ/ρ for various discrete altitudes. The data points are all taken from the aforementioned laboratory measurements. The measured intensities have been normalized on the basis of the known branching ratios for the chosen isotope. As expected, the normalized intensities fall off exponentially with μ/ρ. For any satellite-acquired data the existence of a single straight line provides a ready indication that the debris is all located at effectively one altitude. If the debris is distributed in altitude the data would form a curved line as depicted in Figure 5. In this case one can break up the measured intensity versus μ/ρ curves with three exponentials, corresponding to equivalent debris locations at altitudes of 24 km, 30 km and $\geq$ 60 km with relative weighting factors of 5, 2 and 1, respectively. With the use of several gamma lines, these simple illustrated examples can be extended to provide the debris intensities at several altitudes. Such information can be derived from the simultaneous solution of N equations in N unknowns, a relatively simple and straightforward problem for a digital computer.

Laboratory measurements and calculations are being made in order to arrive at an optimum shielding and collimation geometry for the germanium spectrometer. These activities have included measurements of the response of a 25cc Ge(Li) detector to fission-product gamma rays under various shielding conditions and with the addition of anti-coincidence counters. The final design will represent a tradeoff between the desire for a good directional response and the need to minimize the weight requirements. In the

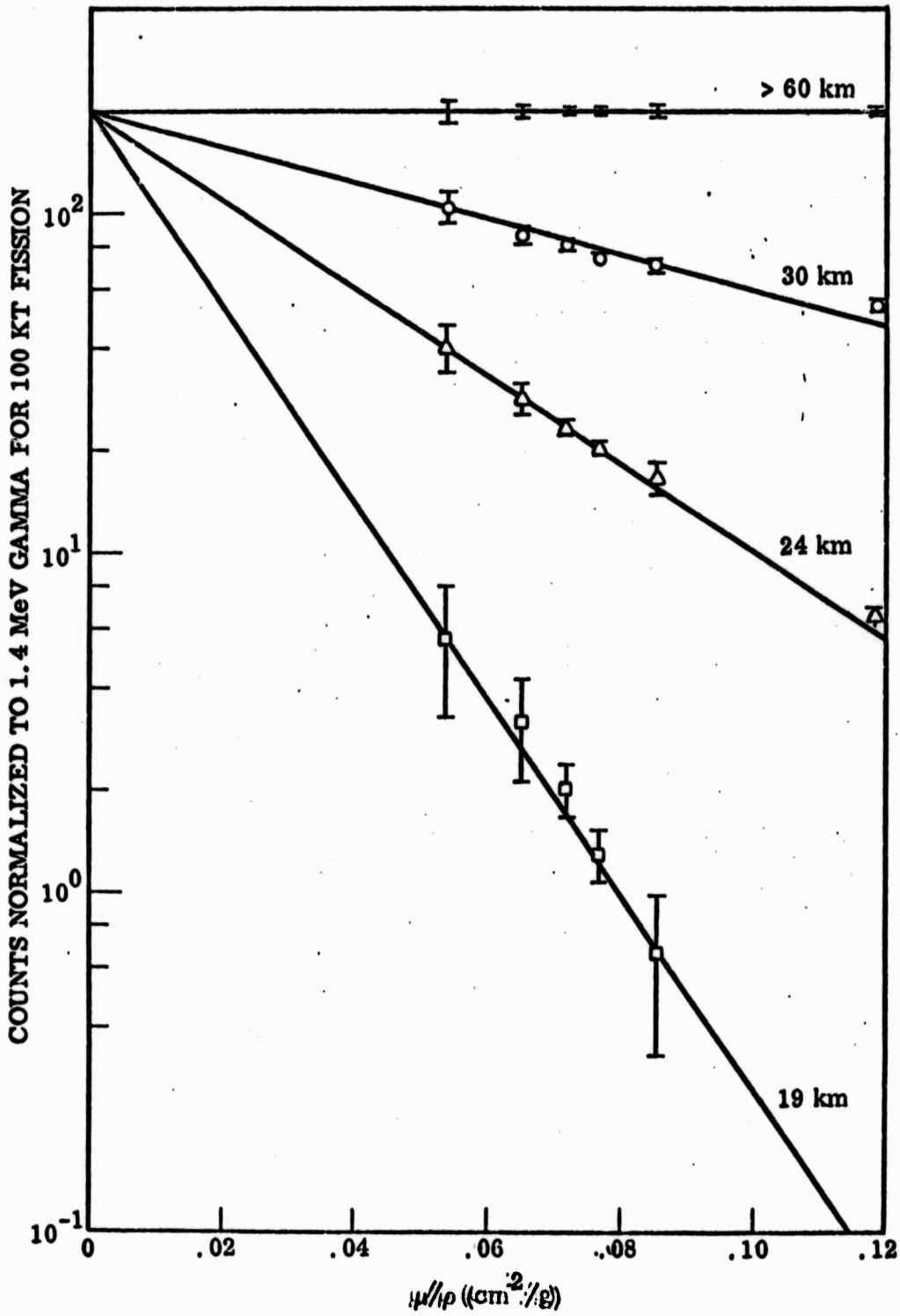

Figure 4 The normalized intensities of six gamma rays from Te^{132}-I^{132} plotted at their corresponding μ/ρ values for four different altitudes.

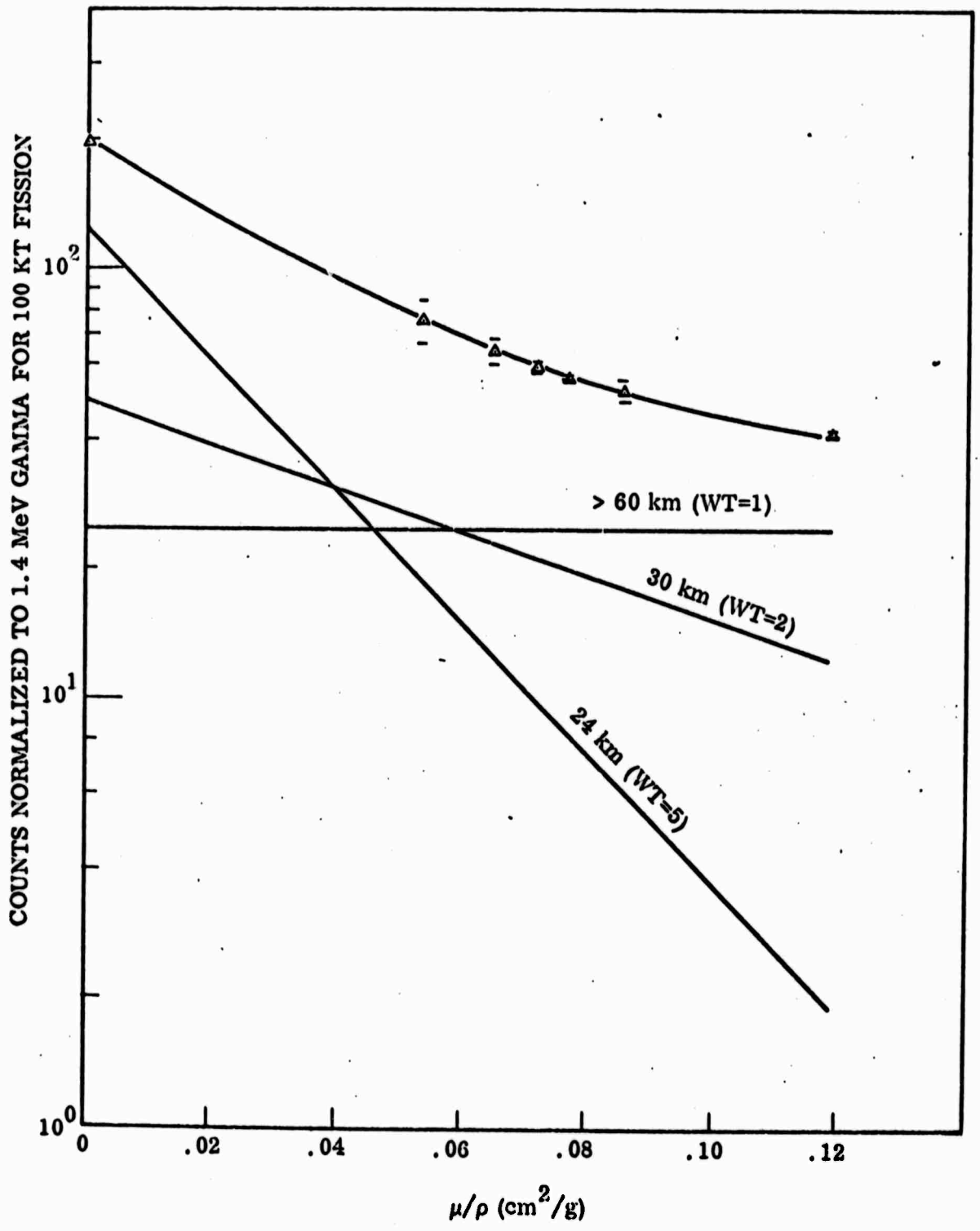

Figure 5 The normalized intensities of six gamma rays from Te^{132}-I^{132} plotted at their corresponding μ/ρ values. The combined intensity versus μ/ρ curve is broken up into the three combined exponentials.

smaller instrumentation package being developed for the preliminary flight we are considering possible methods of supplementing the Ge(Li) spectrometer with more detailed directional coverage obtained from an array of simpler scintillation or solid-state instruments. However, with silicon detectors and plastic scintillation counters, good angular response is difficult to achieve with limited shielding mass. Various experimental arrangements of detectors and shielding geometries are being tested.

We have been evaluating the optimum temperature for operation of Ge(Li) detectors on board a satellite. In the laboratory these detectors are normally kept at liquid nitrogen temperature. In a satellite the use of a liquid coolant is less desirable, so various solid cryogens have been considered. The more attractive of these coolants provide operation at temperatures somewhat above the liquid nitrogen temperature of $77^{\circ}K$. Consequently, the selection of an operating temperature has represented a tradeoff between the general improvement in resolution with decreasing temperature and the engineering advantages of using cryogens in the temperature range of $\sim 100^{\circ}K$ to $\sim 135^{\circ}K$. The performances of germanium counters at elevated temperatures display significant variations from detector to detector. However, laboratory measurements have indicated that large volume Ge(Li) detectors which display good resolution and good diode characteristics at liquid nitrogen temperature will still perform with adequate resolution at temperatures as high as $140^{\circ}K$ to $150^{\circ}K$. On the basis of these measurements we are performing a detailed design study and laboratory evaluation of a solid CO_2 cryogen system operating the detector at a temperature of $\sim 135^{\circ}K$. The tradeoffs between the use of solid CO_2 and the cooler ($\sim 100^{\circ}K$) but otherwise somewhat less attractive solid ethylene cryogen are being studied.

A preliminary design for the solid cryogen cooler required to maintain the lithium-drifted germanium detector at temperatures $< 135^{\circ}K$ has been completed. This selected design allows considerable flexibility in mission lifetime and detector operating temperatures when considering many of the possible design and operational contingencies. The design incorporates an assembly

procedure that eliminates many of the tedious detector module-refrigerator interface problems brought about by the requirement that the detector be maintained at temperatures $\leq 200^{\circ}K$ once drifting has been completed.

In the preliminary design, shown in Figure 6, the refrigerator is ~ 14.25 inches in diameter. This system will provide a maximum one year of in-orbit cooling of the detector at $\sim 135^{\circ}K$ using solid CO_2 as a cryogen. The design has considerable flexibility in that changes in detector temperature requirements and/or the detector module heat loads do not render the refrigerator design unusable. Figure 7 shows that if detector temperatures around $100^{\circ}K$ are found to be necessary, the same refrigeration design can be used for solid ethylene in place of solid carbon dioxide as the cryogen with a resulting reduction of mission lifetime to six months.

The best refrigerator mechanical design is not necessarily the optimum thermal design. For this reason careful attention has been given to a mechanical configuration which will meet the required launch and orbit loads and still minimize the heat loads. All support members in this design were sized to support a 30g launch environment.

The cryogen tank is supported from the vacuum container flange using a fiberglass-epoxy support tube with a minimum wall thickness and a maximum length (see Figure 6). Fiberglass-epoxy was used as the tube material because of its optimum thermal/mechanical characteristics. The entire cryogen tank is surrounded with ~ 2.0 inches of multi-layer insulation and the complete package is in turn mounted in a vacuum container. Vacuum access to the refrigerator is made through a vacuum access port located at the bottom of the vacuum container. The detector module penetration is made through a vacuum quick disconnect located on the refrigerator's top flange.

The detector is supported in its module using three nylon filaments which provide horizontal support. Vertical support is afforded by the copper thermal link. The nylon or dacron filaments were found to have optimum mechanical/thermal characteristics as required by the detector support system. The preliminary detector module design incorporates a vacuum system separate from the refrigerator vacuum system. The module vacuum container extends around the tungsten shielding and thermal link to the refrigerator

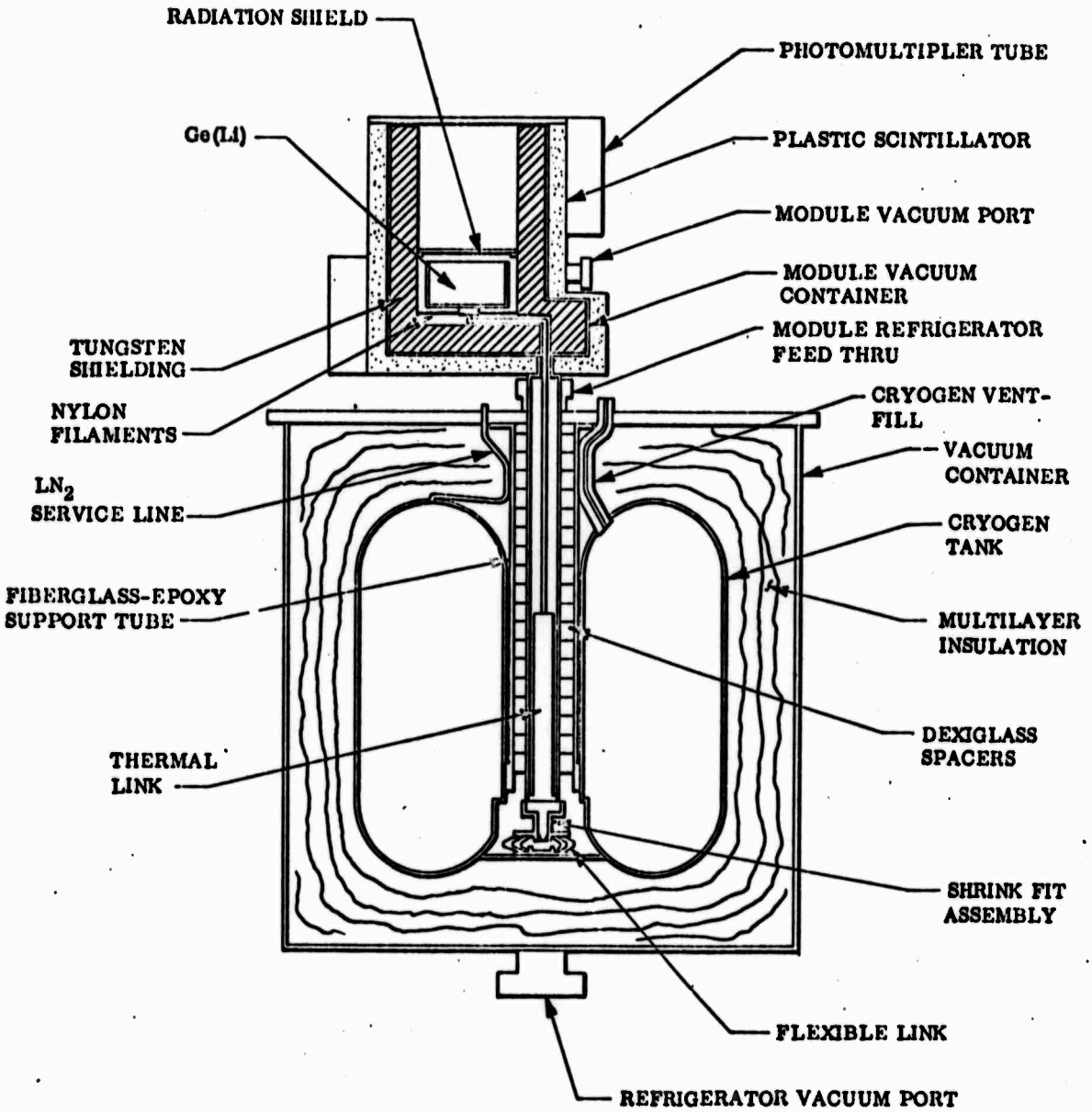

Figure 6 Refrigerator Detector Module Schematic

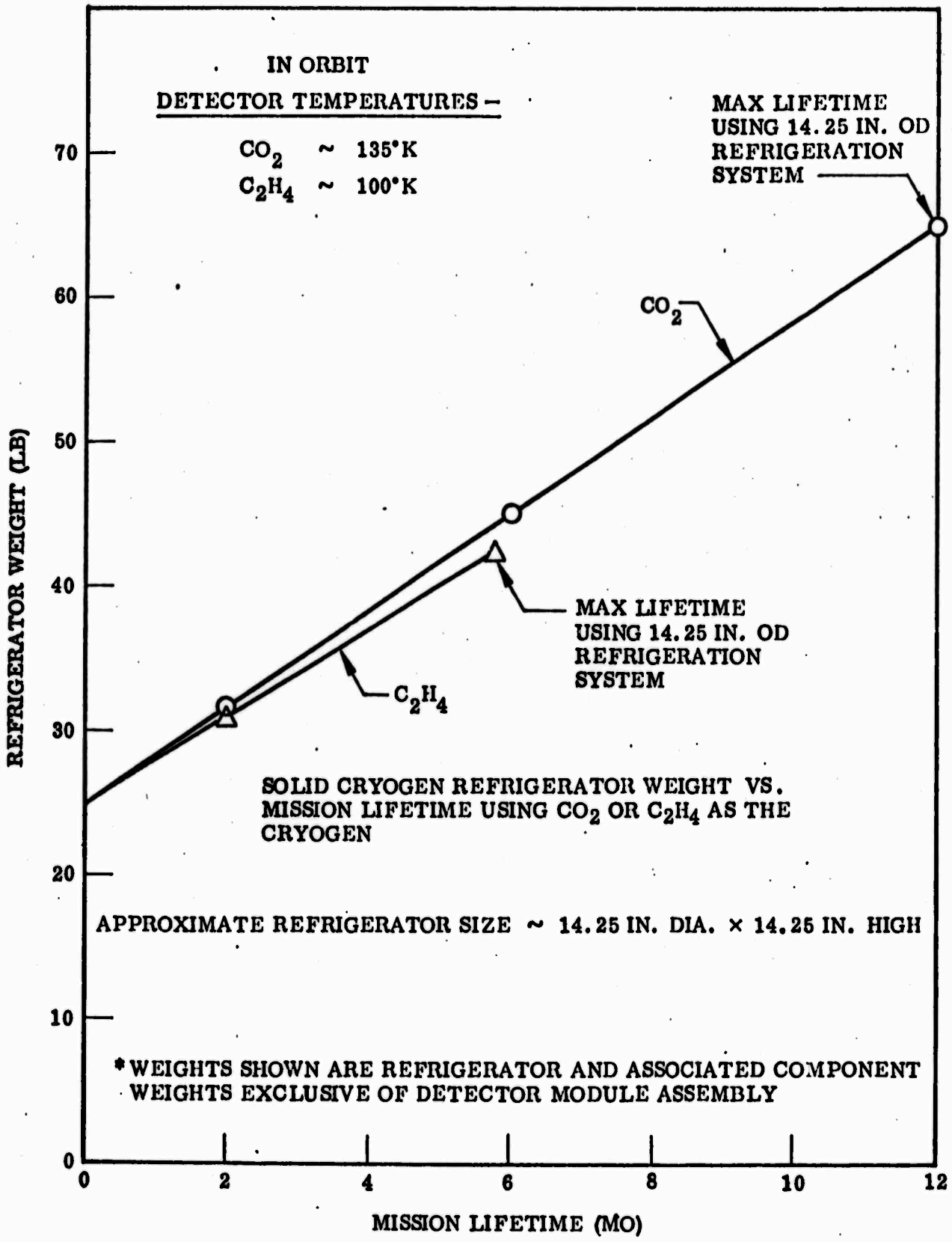

Figure 7 The refrigerator weight (in pounds) plotted as a function of the mission lifetime (in months).

interface point. A separate vacuum container prevents cryodeposition of contamination from the refrigerator's multi-layer insulation system on the cooled thermal link and detector. Such deposits could seriously degrade the thermal performance of the system by raising the emittance of these cooled surfaces.

The interface between the detector module thermal link and the cryogen tank occurs at the shrink fit assembly (see Figure 6). This assembly was developed to facilitate connection of the detector module and refrigerator without disturbing the refrigerator's insulation system or allowing the detector to warm appreciably during assembly. The detector must be maintained below $\sim 200^{\circ}K$ to prevent lithium from diffusing out of the compensated region of the germanium crystal. The shrink fit assembly has been built and tested at the required operating temperatures and found to be feasible to assemble. It maintains its required strength during pull tests conducted between $77^{\circ}K$ and $150^{\circ}K$ after several cycles from $300^{\circ}K$ to $77^{\circ}K$. The pull-apart point of the assembly was $\sim 200^{\circ}K$ which is a significant factor if module removal is ever required.

Table I shows the heat loads on the $130^{\circ}K$ solid CO_2 refrigerant. The high-temperature boundary in all heat load computations was considered to be $\sim 300^{\circ}K$. The heat loads listed in Table I are either conduction or radiation loads with module and refrigerator loads being shown separately. All radiation loads were calculated assuming low emittance "Lockspray" gold surfaces. The heat loads shown in Table I are preliminary only. They apply to the refrigeration scheme shown in Figure 6. In the final thermal design it is hoped that some of these loads can be reduced by thermal techniques requiring laboratory testing to prove their feasibility and to determine their thermal and mechanical effects.

A detector module is being fabricated using a dummy detector for thermal and structural testing. Since a large portion of the heat load and most of the complications present in the proposed refrigeration system are attributable to the detector module, module testing will be conducted before interfacing with the refrigerator. These tests will be conducted using a guarded liquid nitrogen dewar. In this fashion radiation shields and other heat load

TABLE I

Heat Load Summary
One-Year Lifetime CO_2 Refrigerator

	Mode of Transfer	Heat Load (mW)	Comments
MODULE	Conduction		
	Thermal Link Vacuum Container	17	9" long x 0.030" wall x 0.75" diameter fiberglass epoxy.
	Support Wires	5	3 - 0.038" diam. x 1" long nylon filaments
	Radiation		
	Detector	74	2.125" x 1.4" cylindrical detector package
	Thermal Link	15	Two-section copper link Section (1) 0.16 dia. x 6" long Section (2) 0.49" dia. x 6" long Link $\Delta T = 3^{\circ}K$
	Module Total	111	
REFRIGERATOR	Main Support Tube	78	2.0" diam. x 0.075" to 0.050" tapered wall thickness fiberglass epoxy tube 10" long.
	Fill & Vent Lines	25	Convoluted Teflon lines
	Multi-layer insulation	134	2.0" multilayer insulation
	Refrigerator Total	237	
	System Total	348	

reducing techniques can be tested and their feasibility evaluated without involving the additional complications arising when the module is interfaced with the refrigerator.